Low analytical totals in EPMA of hydrous silicate glass due to sub-surface charging: Obtaining accurate volatiles by difference

Ery C. Hughes[1,*], Ben Buse[1], Stuart L. Kearns[1], Jon D. Blundy[1], Geoff Kilgour[2], and Heidy M. Mader[1]

1 School of Earth Sciences, University of Bristol, Wills Memorial Building, Queens Road, Bristol BS8 1RJ, United Kingdom

2 GNS Science, Wairakei Research Centre, 114 Karetoto Road, RD4, Taupo 3384, New Zealand

* Corresponding author. Email: ery.hughes@bristol.ac.uk

Abstract

The major and minor element chemistry of silicate glass is commonly measured using electron probe micro-analysis (EPMA). The volatile content (H_2O ±CO_2) can, additionally, be quantified using 'volatiles by difference' (VBD), but a review of literature data shows that this method consistently overestimates the volatile content. We propose that sub-surface charging during EPMA reduces analytical totals, consequently elevating VBD. Sub-surface charging produces an internal electric field due to trapped implanted electrons, resulting in fewer X-rays being generated and their depth of generation being shallower. The maximum electric field strength required to produce the observed overestimation of VBD is calculated to be ~10^{-1} V·nm^{-1}. Crystals are often used as standards for glass analysis but, as amorphous materials have more defects in the band gap, glasses can trap more electrons resulting in greater amounts of sub-surface charging. As this is not included in matrix corrections, it causes errors for glass analyses, but not for crystal analyses. By calibrating VBD using hydrous glass standards, the effect of charging can be incorporated, and volatile contents can be determined to an accuracy of ±0.1 wt.%, compared to overestimation by ~1 wt.% using conventional VBD methods.

Keywords: Electron probe micro-analysis (EPMA), volatiles by difference (VBD), silicate glass, sub-surface charging, water, Monte Carlo.

Highlights

- Literature data overestimates volatiles in silicate glass using volatiles by difference method (VBD)
- Silicate glass with >2 wt.% volatiles are overestimated by ~1 wt.% on average
- Sub-surface charging decreases X-ray intensity and analytical totals, increasing VBD
- Using glass standards to calibrate VBD achieves accuracy of ±0.1 wt.%

1 Introduction

Electron probe micro-analysis (EPMA) is a critical technique for analysing the composition of silicate glass in volcanology and petrology, such as in melt inclusions and interstitial glass (e.g., Faure and Schiano, 2005). Major and minor element concentration changes, which can be quantified directly using EPMA, provide information on the diversity of magmas (e.g., primary magma composition and mixing events prior to eruption) and their pre-eruptive crystallisation history (e.g., Kent, 2008; Michael and Cornell, 1998). Glass composition can be used in combination with mineral chemistry to test for equilibrium conditions (e.g., Fe-Mg exchange between melt and olivine, Roeder and Emslie, 1970) and estimate magma pressures and temperatures (e.g., olivine-, feldspar-, and pyroxene-melt thermobarometry, see Putirka, 2008, for a review). However, the concentration of the key volatile components (H_2O and CO_2) that have a profound effect on the physical properties of melts (density and viscosity, e.g., Giordano and Dingwell, 2003; Ochs and Lange, 1999), phase relations (e.g., Feig et al., 2006), degassing and eruptive style (e.g., Métrich and Wallace, 2009), cannot be easily and directly determined by EPMA. This shortcoming limits significantly the utility of EPMA in understanding volcanic processes.

One approach to this issue is to estimate the H_2O+CO_2 content of silicate glass by EPMA using the indirect "volatiles by difference" (VBD) method, whereby the discrepancy between the analytical total for measurable (major and minor) elements and 100 wt.% provides an estimate for the total volatile content (Blundy and Cashman, 2008; Devine et al., 1995; Humphreys et al., 2006; King et al., 2002; Nash, 1992). Many trace elements are not analysed by EPMA and if they occur in high abundances will lead to an underestimation of the total. Typically, individual major elements are measured to ~1 % relative error, which results in a ±0.5–0.7 wt.% error on VBD, corresponding to a combination of the errors on individual elements

(Devine et al., 1995; Humphreys et al., 2006). The volatile component by VBD cannot be separated into H_2O and CO_2 but, as H_2O is an order of magnitude more soluble in silicate melts than CO_2, most of the VBD is H_2O. The VBD method has been used widely to quantify the volatile content of experimental samples (e.g., Botcharnikov et al., 2008; Di Carlo et al., 2006; Erdmann and Koepke, 2016) and natural samples such as melt inclusions (e.g., Holtz et al., 2004; Métrich et al., 2004; Rutherford and Devine, 1996; Sommer, 1977).

There are a variety of techniques that can directly and precisely analyse H_2O and CO_2 in silicate glass, such as SIMS, FTIR and Raman (e.g., Hauri et al., 2002; Newman et al., 1986; Thomas, 2000). For comparison, EPMA has higher spatial resolution than SIMS and FTIR (~5 μm diameter using EPMA compared to ~15 μm for SIMS or ~100 μm for FTIR) and is more widely accessible (and less expensive) than SIMS. Also, EPMA does not suffer from problems due to fluorescence or the presence of nanolites which can effect quantification using Raman (e.g., Di Genova et al., 2017b). Therefore, EPMA is often used to estimate H_2O when other techniques are unavailable and, uniquely, provides the complete major and minor element glass chemistry in a single analysis.

A review of literature data (n = 524, see Supplementary Material for complete dataset) of VBD compared to "measured volatile content" (H_2O, and CO_2 where available) is summarised in Table 1 and Figure 1. In these studies, H_2O concentration is measured using FTIR, SIMS, Karl-Fischer titration, or assumed in accordance with experimental conditions (e.g. solubility), whilst CO_2 concentration is measured using SIMS or FTIR (Table 1). Errors are not shown but are typically <10 % relative for measured volatile contents and <0.7 wt.% for VBD. Most (n = 287) of the data is for measured volatile contents <2 wt.%, with slightly fewer (n = 226) analyses of volatile-rich glasses with 2–6 wt.%. There are very few data (n = 11) for glass with >7 wt.% measure volatile content. If VBD and measured volatile content agreed, the data would be evenly distributed around the 1-to-1 trend (Figure 1a), with equal number of analyses under- and overestimating the measured volatile content (Figure 1c). Instead, most of the data lie above the 1-to-1 trend (Figure 1a), with more analyses (>50 %) overestimating the measured volatile content (Figure 1c). This indicates a systematic error, which is not necessarily obvious in small datasets. Including all data (n = 524), the volatile content is overestimated in 63.5 % of analyses (mean overestimation 0.41 wt.% with one standard deviation, 1σ, 1.16 wt.%). For data with measured volatile contents < 2 wt.% (n = 287), VBD overestimates the volatile content in 54.7 % of analyses (mean overestimation 0.08 wt.%, 1σ 0.72 wt.%) (Figure 1b). For measured volatiles > 2 wt.% (n = 237), overestimation occurs in 74.3 % of analyses (mean

overestimation 0.81 wt.%, 1σ 1.43 wt.%). Either EPMA VBD overestimates the true volatile content, or techniques such as SIMS, FTIR or Karl-Fischer titration underestimate the true volatile content. As a variety of different techniques are used to quantify the measured volatile content in these literature data, it seems unlikely that all these techniques would underestimate the true volatile content to the same degree. Hence, it is considered more likely that VBD consistently overestimates the true volatile content.

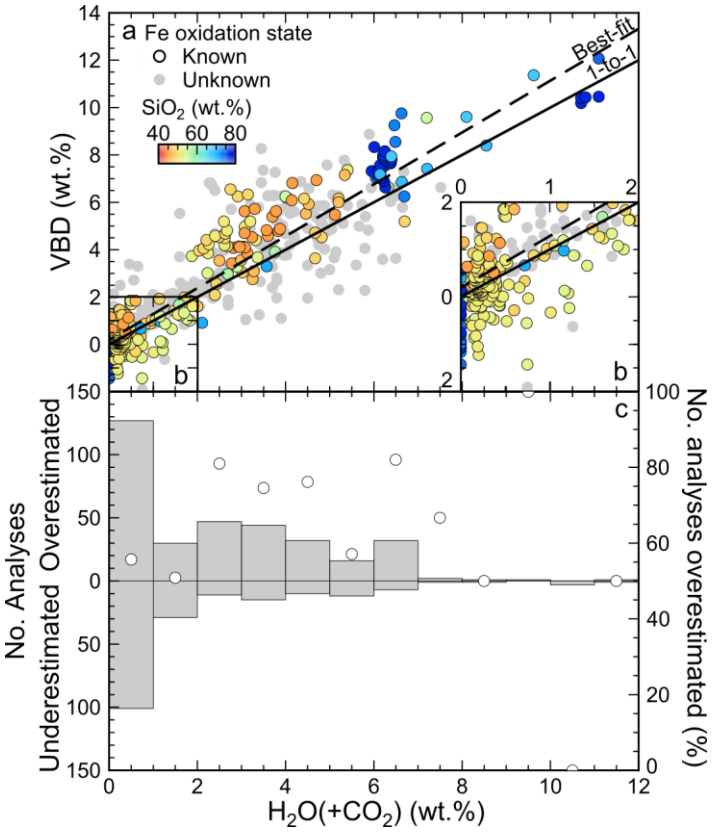

Figure 1. (**a**) Volatiles by difference (VBD) calculated using EPMA against measured volatile content (H_2O, and CO_2 where available). Where Fe oxidation state is known, analyses are coloured by SiO_2 concentration. The solid line indicates the 1-to-1 trend and the dashed line the best-fit to all data (where Fe oxidation state is both known and unknown). (**b**) An expansion of the data from (**a**) at low volatile contents. (**c**) Histogram, binned by measured volatile content, showing the number of VBD analyses that over- and underestimate the measured volatile content on the left-hand axis, and the proportion of VBD analyses that overestimate the measured volatile content (white circles) on the right-hand side axis. Dataset includes 524 analyses, which are available in full in the Supplementary Material.

Table 1 Literature data to compare VBD and measured volatiles.

Study	Composition	*n*	Method			Measured volatiles (wt.%)		Average overestimation (wt.%)
			H_2O	CO_2	Fe^{2+}/Fe_T	Range	Mean ± 1σ	
Natural								
Cottrell and Kelley (2011)	Basalt	59	FTIR	n.d.	μXANES	0.02–0.76	0.28 ± 0.15	-0.05 ± 0.54
Nichols et al. (2002); Shorttle et al. (2015)	Basalt	62	FTIR	n.d.	μXANES	0.12–0.40	0.22 ± 0.07	0.04 ± 0.37
Kelley and Cottrell (2009)	Basalt to basaltic andesite	37	FTIR, SIMS	FTIR, SIMS	μXANES	0.14–5.40	1.52 ± 1.30	-0.03 ± 1.05
Naumov et al. (2008)	Rhyodacite	16	SIMS	n.d.	n.d.	0.90–6.68	4.56 ± 1.60	0.16 ± 0.82
Blundy et al. (2010)	Dacite to rhyolite	38	SIMS	SIMS	n.d.	0.09–6.11	1.68 ± 1.55	0.42 ± 0.77
Chabiron et al. (2001)	Rhyolite	9	SIMS	n.d.	n.d.	0.57–3.73	1.92 ± 0.90	0.06 ± 0.32
Delaney and Karsten (1981)	Rhyolite	11	SIMS	n.d.	n.d.	0.20–3.70	1.92 ± 1.75	0.17 ± 0.91
Drew et al. (2016)	Rhyolite	11	FTIR	FTIR	n.d.	2.27–5.33	4.20 ± 0.89	2.15 ± 1.65
Gurenko et al. (2005)	Rhyolite	12	SIMS, Raman	n.d.	n.d.	1.70–6.50	4.78 ± 1.29	-2.22 ± 0.74
Naumov (2011)	Rhyolite	15	SIMS	n.d.	n.d.	0.07–6.40	1.86 ± 2.16	1.31 ± 1.47
Smith et al. (2010)	Rhyolite	25	SIMS	SIMS	n.d.	0.74–7.52	4.32 ± 1.62	1.17 ± 1.61
Webster and Duffield (1991)	Rhyolite	19	SIMS	n.d.	n.d.	0.40–2.70	1.07 ± 0.63	-0.09 ± 0.77
Webster et al. (1995)	Rhyolite	27	SIMS	n.d.	n.d.	1.60–6.50	3.77 ± 1.16	0.99 ± 1.69
Webster et al. (1996)	Rhyolite	24	SIMS	n.d.	n.d.	0.20–3.60	1.34 ± 1.11	0.41 ± 0.34
Experimental								
Botcharnikov et al. (2005)	Ferrobasalt	16	FTIR	n.d.	Mössbauer	0.72–4.82	2.23 ± 1.42	-0.03 ± 0.41
Lesne et al. (2011)	Basalt	20	SIMS, FTIR	SIMS, FTIR	Titration	1.88–3.32	2.59 ± 0.40	2.14 ± 0.65
Melekhova et al. (2015)	Basalt	11	SIMS	n.d.	μXANES	0.60–7.20	4.27 ± 1.91	1.13 ± 0.97
Stamper et al. (2014)	Basalt	25	SIMS	SIMS	μXANES	0.03–5.20	2.98 ± 1.53	1.24 ± 1.53
Di Genova et al. (2014, 2013)	Latite, basalt, pantellerite	13	KFT	n.d.	Titration	0.02–6.32	1.99 ± 1.81	-0.13 ± 0.40
Riker et al. (2015)	Dacite	8	SIMS	SIMS	μXANES	6.14–9.63	7.42 ± 1.22	0.71 ± 0.85
Wilke et al. (2002)	Dacite	5	KFT	n.d.	Mössbauer	10.70–11.10	10.88 ± 0.20	-0.17 ± 0.65

Devine et al. (1995)	Rhyolite	10	SIMS, FTIR	n.d.	n.d.	0.16–6.38	3.11 ± 2.31	0.14 ± 0.36
Di Genova et al. (2017)	Rhyolite	11	*	n.d.	Titration		0	-0.50 ± 0.66
Zhang et al. (1997)	Rhyolite	8	FTIR	n.d.	n.d.	0.75–5.40	2.18 ± 1.69	0.14 ± 0.21
	Metaluminous -					5.95–6.63	6.23 ± 0.16	1.47 ± 0.64
Gaillard et al. (2001)	peralkaline rhyolite	23	FTIR	n.d.	Titration			
Di Genova et al. (2016)	Pantellerite	9	*	n.d.	Titration		0	-0.55 ± 0.45

Notes: *n* refers to the number of analyses in each study; n.d. means not determined, * assumed due to experimental conditions; for measured volatiles, the range of the study is given followed by the average ± one standard deviation (1σ) in brackets; and the average overestimation is the average of (VBD – measured volatiles) for each study ± 1σ. The complete dataset is available in Supplementary Material.

Evidently, VBD is accurate at low volatile contents (<2 wt.%), but consistently overestimates the volatile content in volatile-rich glass (>2 wt.%) by nearly 1 wt.%. Such large discrepancies would have significant impact on the calculated physical and chemical properties of the melt and, in turn, its behaviour before and during volcanic eruptions. For instance, a 1 wt.% overestimation in H_2O concentration could change the calculated entrapment pressure of water-saturated melt inclusions by up to ~50 MPa, equivalent to ~2 km depth change (Newman and Lowenstern, 2002). Similarly, Di Genova et al. (2013) calculate that the viscosity difference between 2.5 and 4.0 wt.% dissolved H_2O is approximately an order of magnitude ($10^{2.4}$ to $10^{3.3}$ Pa·s at 1023 K). Therefore, it is important to understand the cause of the overestimation of VBD and to develop a method to improve the accuracy of VBD measurements.

2 Volatiles by difference using electron probe micro-analysis

EPMA uses the intensity of characteristic X-rays, generated by bombarding a sample with an electron beam, to measure its composition. Typically, *K*α X-ray lines are used for quantification of elements with atomic number < 30, as they have the highest intensity of X-rays emitted from a specific atom. *K*α X-rays are generated by an incident electron ejecting an electron from the innermost shell (*K* shell) of a target atom, which is replaced by an electron from the shell above (*L* shell), emitting the *K*α X-ray. Element concentrations are calculated by comparing the intensity of X-rays emitted by standards of known composition to those emitted by the unknown. Emitted X-ray intensity depends on the number of X-rays generated and how much absorption and fluorescence occurs as they travel through the sample, which in turn depend on the sample composition. Matrix corrections are used to account for differences in composition between the standards and unknowns that would affect mean atomic number, absorption and fluorescence. As oxygen, a very important component of silicate glass, is not typically measured during EPMA, element concentrations are treated as oxide components, with the amount of oxide calculated stoichiometrically from the element at the assumed valence state. Glass is an insulator and therefore builds-up sub-surface charging during analysis as electrons become trapped within the sample (Bastin and Heijligers, 1991). This causes element migration, as ions are displaced in response to the build-up of charge at depth, and changes the generation and emission of X-rays (Cazaux, 1996). These potential causes for discrepant VBD analyses are addressed individually below.

2.1 Converting to oxides: Oxidation state of multi-valent elements

The valence state of the cation species in the glass must be known in order to calculate oxygen using stoichiometry. If oxygen itself is measured, the excess oxygen not required stoichiometrically by other elements can be used to calculate the unmeasured volatile component. For most elements in natural silicate glass there is a single valence state, but Fe and S can have multiple oxidation states, e.g. Fe can be present as FeO, Fe_2O_3, or a mixture of both. Per Fe atom, Fe_2O_3 is ~10 % heavier than FeO which results in a ±5 % relative error in oxide concentration when converting from elemental Fe if the oxidation state is unknown. This is important for basalts which contain 5–14 wt.% FeO_T (FeO_T = all Fe reported as FeO), as the uncertainty in the amount of oxygen assigned to Fe leads to a ±0.3–0.7 wt.% error in VBD. Consequently, to obtain reliable VBD, an independent constraint on Fe oxidation state is required (Donovan and Vicenzi, 2008; Nash, 1992). Rhyolites typically contain only 1–4 wt.% FeO_T, therefore the uncertainty from the amount of stoichiometric oxygen assigned to Fe is small (±0.1–0.2 wt.%), and has a correspondingly smaller effect on VBD error. For rhyolites, therefore, an independent constraint on Fe oxidation state is less critical.

As the Fe oxidation state is important in estimating VBD for silicate glass containing significant Fe, only data with measured Fe oxidation state are included in our compilation of published glasses with FeO_T > 2 wt.% (e.g., basalts and pantellerites). In these cases, the measured Fe oxidation state is used to assign FeO_T into FeO and Fe_2O_3 to calculate VBD. Where FeO_T < 2 wt.% (e.g., rhyolites) the data are included even when no independent measurements of Fe oxidation state are available. At high concentrations sulphur oxidation state will also impact the analytical total, and therefore VBD. At S < 2500 ppm, the error due to the uncertainty in sulphur speciation (S^{2-} to S^{6+}) is < ±0.2 wt.%. If no Fe oxidation state is available and when S is reported, VBD is calculated assuming all Fe is Fe_2O_3 and all S is SO_3. Such VBDs represent a minimum estimate.

2.2 Matrix corrections

The matrix correction accounts for differences in mean atomic number, absorption and fluorescence of X-rays for samples with different compositions. If the unmeasured volatile is not included in the matrix correction for analyses without measured oxygen, the mean atomic number used for the matrix correction is incorrect and absorption by oxygen is underestimated. This can lead to analytical totals being underestimated by ~1 wt.% (Devine et al., 1995;

Donovan and Vicenzi, 2008; Roman et al., 2006). This is corrected for by calculating the unmeasured volatiles (typically specified as H_2O) by difference within the matrix correction routine (Donovan and Tingle, 1996).

2.3 Element migration

Silicate glass can become unstable during EPMA due to the diffusive migration of mobile elements (e.g., Na), sometimes referred to as 'beam damage' (e.g., Nielsen and Sigurdsson, 1981). Glass composition controls the severity of beam damage and hydrous glass is more susceptible than anhydrous glass (e.g., Hughes et al., 2018; Humphreys et al., 2006; Zhang et al., 2018). Element migration can also occur in hydrous minerals, such as amphibole and apatite, causing errors in VBD estimates of these minerals (e.g., Stock et al., 2015). Beam damage is accompanied by a corresponding increase in the concentration of immobile elements (e.g., Si and Al) referred to as "grow-in" (e.g., Morgan and London, 2005; Nielsen and Sigurdsson, 1981). These problems can be corrected for by monitoring the X-ray intensity over time and extrapolating back to the initial value (Nielsen and Sigurdsson, 1981), often referred to as "time-dependent intensity" (TDI) corrections. As the change in X-ray intensity with time is not necessarily linear, only elements measured at the onset of the analysis can be corrected for (one per spectrometer, or typically five out of the twelve commonly analysed elements). Therefore, it is important to measure first those elements that are likely to diffuse or grow-in. Measuring mobile elements first and for short times, even where the TDI correction is not required, is now routinely employed to address this problem (e.g., Blundy and Cashman, 2008)

2.4 Sub-surface charging

Electrical insulators (e.g., silicate crystals and glasses) have a large band gap, which is the energy difference between the valence and conduction bands where no electrons can reside. Hence, for insulators a large amount of energy is required to promote an electron from the valence band into the conduction band. For electron imaging and EPMA, insulator materials are routinely coated with a thin conductive layer, typically carbon, to prevent surface charging. The conductive coat does not, however, prevent *sub-surface* charging, whereby incident electrons are trapped within the sample (Cazaux, 1996). Charge is trapped as electrons

occupying energy levels in the band gap produced by defects, such as a vacancies, interstitial atoms or substitutions within the lattice structure.

Trapped electrons generate an electric field within the sample, which enhances the deceleration of electrons as they pass through the sample. Hence, X-ray ionisations are reduced and generated closer to the surface and undergo less absorption. This is reflected in the change in calculated φ(ρZ) curves, which depict intensity variations in X-ray generation and emission with depth relative to a thin film (e.g., Figure 2), by an internal electric field (Cazaux, 1996). The resulting measured X-ray intensity is a trade-off between these two effects. For low energy X-rays, e.g. O*K*α, where X-ray absorption by the matrix is reduced, emitted X-ray intensity may increase, but for most higher energy X-rays intensity will fall as a consequence of charge trapping.

Charge-trapping sites, (i.e., defects in the band gap) are more common in amorphous materials than in single crystals (Bonnelle, 2004)~~,~~. Therefore, the magnitude of sub-surface charging effects is greater in glasses than in crystals, all else being equal. Furthermore, charge trapping is dynamic and can increase as a result of electron beam irradiation (Bonnelle, 2004). Typically, crystalline materials that are stable under the electron beam are used as standards. When these crystalline standards are used for crystal analysis they should experience a similarly small magnitude of charging and no quantification error will be observed. Hence, the issue of sub-surface charging has little impact on the analysis of anhydrous minerals (individual crystals), which typically yield totals of 100±0.5 wt.% when oxygen is calculated by stoichiometry, notwithstanding Fe redox issues described above. Conversely, when crystals are used as standards for glass analysis, the magnitude of sub-surface charging will likely be different, providing a potential explanation for the discrepancy in analytical totals. Sub-surface charging is not included in current matrix corrections, as the amount of charging is difficult to determine. If standards and unknowns experience different amounts of charging during analysis, quantification errors may result.

Direct measurements of sub-surface charging are difficult, but are possible post-irradiation within ground-coated insulators using the pressure wave propagation method (Maeno et al., 1989), thermal pulse method (Cherifi et al., 1992), or electrical methods (Sessler and Yang, 1998). To measure the dynamic build-up of charge, the electrostatic influence method can be used on coated (Jbara et al., 2002) and uncoated (Fakhfakh et al., 2003) samples. Using this technique, maximum electric field strengths (F_{max}) of ~ 1 V·nm^{-1} have been measured in glass

(Jbara et al., 2004, 2002), that would cause significant distortion to the φ(ρZ) curve (Cazaux, 1996; Jbara et al., 1997). Sub-surface charging has been observed indirectly by measuring the migration of alkali elements in glasses over time (e.g., Gedeon et al., 1999; Gedeon and Jurek, 2002; Jbara et al., 1995; Lineweaver, 1963), and by comparing the X-ray intensity of charged and uncharged polycrystalline Al_2O_3 (e.g. Benhayoune and Jbara, 1996; Ghorbel et al., 2005). Using the decay of Na*K*α X-ray intensities over time and measured diffusivities of Na through silicate glass, Jbara et al. (1995) calculated F_{max} of 10^{-4}–10^{-1} V·nm^{-1}. As these magnitudes of sub-surface charging may measurably impact quantitative EPMA, we investigate the effects of sub-surface charging on the analysis of hydrous glass to see whether this additional effect could cause an underestimation of analytical totals and concurrently elevation of VBD.

3 Methods

We modelled the effect of sub-surface charge on glass analysis using the Monte Carlo simulation program Win X-ray (Demers and Gauvin, 2004; Gauvin et al., 2006), which incorporates the charge density model proposed by Cazaux (1996). We then use the results from Win X-ray to calculate the VBD.

3.1 Sub-surface charging model

Sub-surface charging can be modelled using the steady-state sub-surface charging model of Cazaux (1996). This uses a one-dimensional charge distribution, which is valid if the irradiated area is large compared to the maximum penetration depth of electrons and charge builds up instantaneously. The sample thickness must greatly exceed the maximum penetration depth of electrons, and the top and bottom surfaces of the sample must be grounded (Cazaux, 1996; Demers and Gauvin, 2004). In this case, the electric field within the sample is described by:

$$F=[\rho_t(z_{max}-z)]/\varepsilon$$

where F is the electric field strength (V·m^{-1}), ρ_t is the trapped charge density (C·m^{-3}), z_{max} is the maximum penetration depth of electrons (m), z is the depth in the sample (m), and ε is the permittivity of the sample (F·m^{-1}) (Cazaux, 1996). The maximum electric field (F_{max}) occurs at the interface between the sample and the conductive coat (z = 0). The magnitude of the

electric field is thus dependent on both the material properties of the sample and the analytical conditions.

3.2 Win X-ray: Monte Carlo simulation program

The inputs for Win X-ray are sample composition and density (ρ_m), analytical conditions (accelerating voltage, beam current and beam diameter), and maximum electric field (F_{max}). The maximum penetration depth of electrons within the sample (z_{max}), φ(ρZ) curves (generated and emitted), and measured X-ray intensity (I) for the principal characteristic X-rays (e.g., $K\alpha$, $K\beta$, $L\alpha$) of each target element are calculated.

We choose glass St8.1.B from Lesne et al. (2011) as the sample composition as it is a typical basalt. To simplify the composition, all Fe is FeO and volatiles other than H_2O (S, Cl, and CO_2) are excluded. We modelled typical analytical conditions used for silicate glass (15 kV accelerating voltage, 10 nA beam current, and 10 μm beam diameter), with dissolved H_2O concentrations of 0, 5 and 10 wt.%. ρ_m for each H_2O concentration was calculated using density models of melts at room temperature and pressure, which were 2.793, 2.652 and 2.524 ($g \cdot cm^{-3}$) for 0, 5 and 10 wt.% H_2O respectively (Bottinga and Weill, 1970; Lange, 1997; Lange and Carmichael, 1990; Ochs and Lange, 1999; Toplis et al., 1994). We varied F_{max} between 0 and 0.2 $V \cdot nm^{-1}$ for each H_2O concentration, and the maximum penetration depth (z_{max}) was calculated using the Kanaya-Okayama Range (Kanaya et al., 1972). The large beam diameter satisfies the requirement of one-dimensional charge distribution (i.e., charge distribution only varies in z as the irradiated area is large compared to the electron penetration depth). Each simulation was run for one million electrons.

3.3 Calculating VBD from Win X-ray results

X-ray intensities without sub-surface charging (I) were used as standards to derive k-ratios ($k = I'/I$, I' is the X-ray intensity with sub-surface charging) at each H_2O concentration and calculate concentrations when sub-surface charging was imposed ($C' = k \cdot C$, where C is the specified concentration). The measured analytical total and VBD were then calculated. An example calculation is shown in Table 2.

Table 2. Example calculation of modelled oxide concentration (C') by comparing uncharged X-ray intensities (I) to charged X-ray intensities (I'), for F_{max} = 0.20 V·nm^{-1}.

	I	I'	k	C (wt.%)	C' (wt.%)
SiO_2	5.96×10^4	5.85×10^4	0.980	51.86	50.08
TiO_2	7.97×10^2	7.65×10^2	0.960	0.84	0.81
Al_2O_3	1.99×10^4	1.96×10^4	0.983	18.63	18.31
Fe_2O_3	4.52×10^3	4.36×10^3	0.964	8.12	7.83
MgO	4.67×10^3	4.62×10^3	0.990	6.02	5.96
CaO	1.79×10^4	1.72×10^4	0.961	11.11	10.68
Na_2O	7.42×10^2	7.40×10^2	0.997	1.98	1.97
K_2O	2.86×10^3	2.76×10^3	0.963	1.44	1.39
H_2O				0.00	-
Total				100.00	97.78
VBD				0.00	2.22

Notes: Data are available in the Supplementary Material.

4 Results

Figure 2 gives the φ(ρZ) curves of the *K*α lines of interest, in order of increasing X-ray energy from upper left to lower right. Values of the φ(ρZ) function of the emitted curve [φ(ρZ)$_e$] are always less than the generated curve [φ(ρZ)$_g$], as some X-rays are always absorbed. At shallow depths in the sample, φ(ρZ)$_g$ for F_{max} = 0.00 and 0.20 V·nm^{-1} are comparable, but at greater depths, the intensity of generated X-rays falls off more quickly for F_{max} = 0.20 V·nm^{-1}. For Si, Al, Mg and Na calculated values of φ(ρZ)$_e$ for F_{max} = 0.00 and 0.20 V·nm^{-1} are similar, whereas for Ti, Fe, Ca, and K φ(ρZ)$_e$ for F_{max} = 0.20 V·nm^{-1} is noticeably less than for F_{max} = 0.00 V·nm^{-1}.

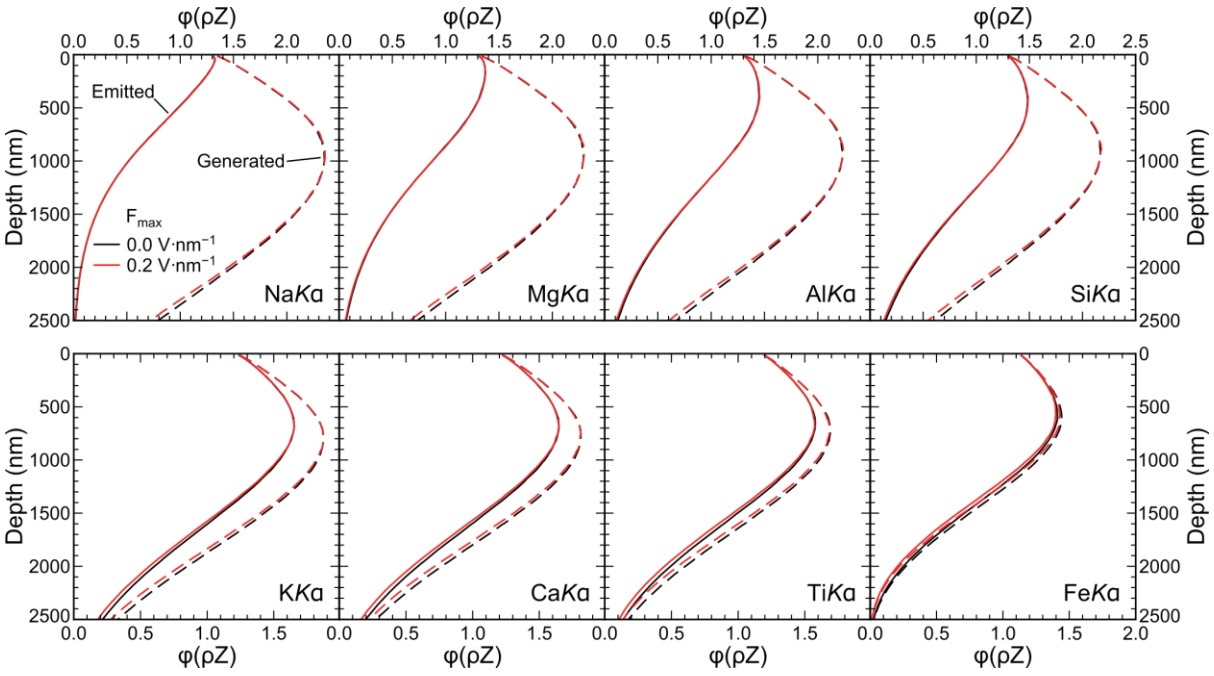

Figure 2. Generated and emitted φ(ρZ) curves against depth for *K*α lines of different elements (in ascending order of X-ray energy, indicated in the bottom right corner) for St8.1.B with 5 wt.% H_2O, for F_{max} = 0.0 (black) and 0.2 V·nm^{-1} (red).

Figure 3 shows that for X-rays with energies > 1 keV k < 1.00, whereas for X-rays with energies < 1 keV, k > 1.00. Measured X-ray intensities are reduced by the presence of an electric field for most elements routinely measured by EPMA (Figure 3). On the other hand, the intensity of heavily absorbed X-rays, such as O*K*α, increases in the presence of an electric field. Broadly, k decreases with increasing X-ray energy, F_{max}, and H_2O concentration of the glass, but does not do so smoothly. The effect of F_{max} and H_2O concentration increases with increasing X-ray energy. For H_2O concentrations of 0 and 5 wt.% k increases for X-ray energies > 5 keV, whereas for 10 wt.% H_2O it does not change. The effect of H_2O concentration on k increases with increasing F_{max}.

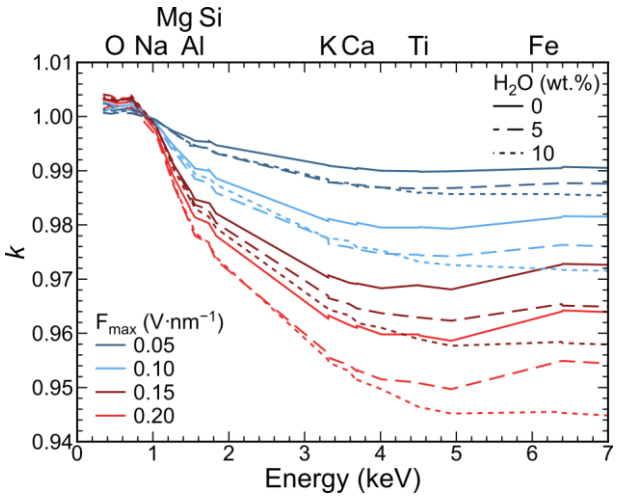

Figure 3. k against X-ray energy with energy of *K*α X-rays for different elements indicated along the top. Different values of F_{max} are shown using different line colours, whilst different glass H_2O concentrations are shown by different line styles. For instance, results using an F_{max} of 0.10 V·nm^{-1} for H_2O = 5 wt.% are shown in the long-dashed, light blue line. Data are available in the Supplementary Material.

Reduction in X-ray intensities means that VBD, calculated using C', is always greater than the specified H_2O (Figure 4). The value of VBD increases with increasing F_{max}, and lines of equal F_{max} appear parallel (Figure 4).

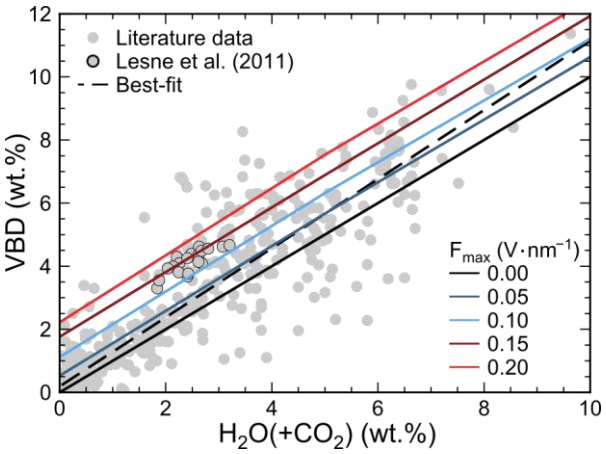

Figure 4. Volatiles by Difference (VBD) calculated using Win X-ray plotted against volatile content, for different F_{max} (line colour). Literature data included for comparison. Data for basalt glass of Lesne et al. (2011) are highlighted.

5 Discussion

5.1 Effect of F_{max}

Modelling results confirm that more low energy X-rays (<1 keV) and fewer high energy X-rays (>1 keV) are emitted when an electric field is present. This is because, although fewer X-rays are generated overall, they are generated at shallower depths reducing X-ray absorption which most affects strongly absorbed, rather than weakly absorbed, X-rays. Moreover, the deceleration of electrons will affect high energy X-rays more than low energy X-rays as the overvoltage (ratio of the accelerating voltage to the critical excitation energy of the X-ray) is smaller; the magnitude of intensity reduction will therefore vary with primary accelerating voltage (Ghorbel et al., 2005). As the *K*α X-rays used for quantification are >1 keV, the presence of an electric field in the glass reduces emitted X-ray intensity (Figure 2 and Figure 3), resulting in low analytical totals and overestimated VBD (Figure 4). Oxygen can be measured to calculate the volatile content, but this would also lead to an overestimation of volatiles because the intensity of O*K*α increases with an electric field present. At constant F_{max}, k decreases with increasing H_2O concentration, which is likely due to the decrease in ρ_m that results from increasing amounts of dissolved H_2O in the glass. For most *K*α lines this effect is small, as reflected in almost parallel lines of modelled VBD at different values of F_{max}.

We can compare our results to the studies of Jbara et al. (2004, 2002, 1995) that irradiated glasses at a 13.0–18.5 kV accelerating voltage, 2–3 nA beam current, and 10^1–10^7 μm^2 irradiated area, giving doses of 10^{-4}–10^2 C·m^{-2}·s^{-1}, similar to those modelled here (~10^1 C·m^{-}

$^{2}\cdot s^{-1}$). The F_{max} we inferred using Win X-ray ($\sim 10^{-1}$ V·nm^{-1}) is in the range measured by Jbara et al., i.e. 10^{-4}–10^{0} V·nm^{-1}.

5.2 Controls on F_{max}

Win X-ray adopts a user-selected F_{max} during simulation, but it is important to understand what might control this value. F_{max} is inversely proportional to ε, and glass has a value of ε_r (relative permittivity, or dielectric constant) of 3–10, which depends on composition, temperature, and frequency. For anhydrous basalt $\varepsilon_r \approx 4.8$ (Carmisciano et al., 2011). Unfortunately, there are no data available for the effect of H_2O concentration on ε_r.

F_{max} is proportional to z_{max}, which increases with decreasing ρ_m and increasing accelerating voltage. ρ_m is a function of glass composition, including H_2O concentration, hence z_{max} and F_{max} increase with increasing H_2O concentration. This is consistent with the increased discrepancy between measured volatile content and VBD at elevated H_2O concentration (Figure 1 and Table 1). For glass with measure volatile content < 2 wt.%, the mean overestimation was 0.08 wt.% (with one standard deviation, 1σ, 0.72 wt.%), whereas for glass with measured volatiles content > 2 wt.% the mean overestimation was 0.81 (1.43 1σ) wt.%.

F_{max} is also proportional to ρ_t. Intrinsic charge-trapping sites are a material property, caused by defects in the band gap (Bonnelle, 2004), which is partly a function of glass composition (Fakhfakh et al., 2010). Bombarding a sample with electrons creates additional charge-trapping sites (Bonnelle, 2004), hence ρ_t is also dependent on analytical conditions, such as beam current. Jbara et al. (1995) found that a constant proportion of charge (relative to the number of incident electrons per unit area, dose), was trapped in glass during analysis. This requires the number of charge-trapping sites to increase linearly with electron dose. Using results from Win X-ray gives a $\rho_t \approx 10^{2}$ C·m^{-3} for our data. The dose rate is $\sim 10^{1}$ C·m$^{-2}\cdot$s^{-1} which means that $\sim 10^{-3}$ % of incident electrons are trapped, an order of magnitude larger than 2.6×10^{-4} % from Jbara et al. (1995) at similar, analytical conditions. The main differences between our study and that of Jbara et al. (1995) are the concentrations of SiO_2 (73 vs. 52 wt.%) and H_2O (0 vs. 1–3 wt.%). In the literature data (Figure 1a), there is no significant difference in the magnitude of charging between glasses of different SiO_2 concentrations. Conversely, glasses with measured volatiles < 2 wt.% appear to suffer little charging whereas those with >2 wt.% are more affected (Figure 1). We conclude that the order of magnitude difference in charge-

trapping proportion between our study and Jbara et al. (1995) is most likely caused by H_2O concentration. Hydrous glass are more unstable during electron beam irradiation (Hughes et al., 2018; Humphreys et al., 2006; Zhang et al., 2018), which could create more charge-trapping sites during analysis compared to anhydrous glass or crystals, and hence increased F_{max}.

5.3 Obtaining accurate VBD

Matrix corrections could include the effects of sub-surface charging on X-ray generation, therefore allowing primary standards that are affected by different amounts of charging (e.g. crystals and anhydrous glass) to be used for calibration (Cazaux, 1996). Unfortunately, this requires accurate calculation of F_{max} in both primary standards and unknowns at the analytical conditions used. As ρ_t depends on composition, structure, and analytical conditions, it must be measured rather than calculated on the primary standards and unknowns during analysis. Such measurements are not routine and there are few data on the effect of composition (especially H_2O concentration) on ε_r, a requisite for calculating F_{max}.

Alternatively, matrix-matched primary standards (i.e., hydrous glasses of appropriate composition) can be used for major element calibration, such that primary standards and unknowns would experience similar amounts of charging. This requires different major element primary standards for each glass H_2O concentration. Currently few, if any, hydrous glass primary standards with independent measurements of composition exist. However, the error on any single element is small and typically within analytical error. Hence in practice only VBD needs to be corrected for the effect of sub-surface charging and this can be done by internally calibrating VBD with a set of well characterised, matrix-matched secondary standards of known volatile content (e.g., Botcharnikov et al., 2008; Di Carlo et al., 2006; Holtz et al., 2004) and Fe (±S) oxidation states. The VBD secondary standards should be analysed using the same analytical and calibration conditions as the unknowns to generate an empirical calibration curve for each session. This will result in similar amounts of charging in the secondary standards as in the unknowns. To produce a reliable calibration curve for VBD, a range of H_2O concentrations covering those expected in the unknowns should be used to avoid extrapolation. Additionally, there must be an independent constraint on the Fe oxidation state (and S if the concentration is high) of the unknowns if they are Fe-rich basalts or pantellerites.

From Figure 4 it can be seen that the Lesne et al. (2011) data have measured VBD data comparable to modelled VBD for $F_{max} \approx 0.1$ V·nm^{-1}. An example of the empirical correction

using these data is shown in Table 3 and Figure 5**Error! Reference source not found.**. Glass composition and S oxidation state were measured by EPMA, Fe oxidation state by wet chemistry, and H_2O and CO_2 concentration by SIMS and/or FTIR. Samples from St8.1.B are used as VBD secondary standards as they cover the widest range in H_2O (1.9–3.1 wt.%), and samples from MAS.1.A and MAS.1.B are treated as unknowns (Table 3 and Figure 5). The average accuracy improves from a consistent overestimate of +1.69 (0.23 1σ) to a slight underestimate of -0.06 (0.32 1σ) wt.%. This demonstrates the viability of using an empirical correction to achieve high accuracy VBD, by accounting for both variations in sub-surface charging and calibration errors.

Table 3 Example VBD correction using data from Lesne et al. (2011).

Sample	Measured volatiles (wt.%)	*s.d.*	VBD (wt.%)	*s.d.*	VBD corrected (wt.%)	*s.d.*
MAS.1.B2[a]	2.21	*0.13*	4.30	*0.40*	2.60	*0.48*
MAS.1.B3[a,b]	2.49	*0.13*	4.39	*0.84*	2.72	*1.01*
MAS.1.B4[a,b]	2.62	*0.13*	4.39	*0.36*	2.70	*0.43*
MAS.1.B5[a,b]	2.26	*0.13*	4.10	*0.52*	2.36	*0.63*
MAS.1.B6	2.41	*0.13*	3.68	*0.73*	1.85	*0.87*
MAS.1.B7[b]	1.84	*0.12*	3.30	*0.75*	1.41	*0.90*
MAS1.A1[a]	2.63	*0.13*	4.62	*0.50*	2.98	*0.60*
MAS1.A2[a]	2.14	*0.13*	3.99	*0.44*	2.24	*0.53*
MAS1.A3[a]	2.68	*0.13*	4.09	*0.57*	2.36	*0.68*
MAS1.A4[a]	2.62	*0.13*	4.15	*0.48*	2.42	*0.57*
MAS1.A5[a]	2.24	*0.13*	3.81	*0.46*	2.01	*0.55*
MAS1.A6	2.42	*0.13*	3.77	*0.88*	1.97	*1.05*
MAS1.A7[a]	2.04	*0.10*	3.93	*0.90*	2.15	*1.08*
St8.1.B2[a]	2.41	*0.13*	4.26	*0.73*	2.55	*0.88*
St8.1.B3[a]	3.07	*0.13*	4.63	*0.51*	2.99	*0.61*
St8.1.B4[a,b]	3.20	*0.13*	4.67	*0.40*	3.05	*0.48*
St8.1.B5[a]	2.67	*0.13*	4.48	*0.57*	2.82	*0.68*
St8.1.B6	2.80	*0.13*	4.56	*0.65*	2.91	*0.78*
St8.1.B7[a]	1.88	*0.14*	3.55	*0.47*	1.70	*0.57*

Notes: Measured volatiles is H_2O (+CO_2) using SIMS and/or FTIR, VBD includes [a]Fe^{2+}/Fe_T and [b]S^{6+}/S_T, and VBD corrected uses an empirical correction based on St8.1.B data such that VBD corrected = (VBD – 2.13)/0.83. The full calculation is available in the Supplementary Material.

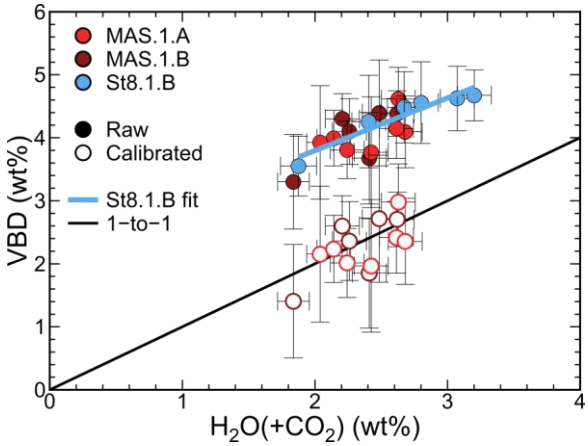

Figure 5 VBD against measured volatiles (H_2O+CO_2) from glasses of Lesne et al. (2011), where VBD includes independent constraints on Fe^{2+}/Fe_T and S^{6+}/S_T. Closed symbols are the raw data and open symbols have been calibrated using a fit to the St8.1.B glasses (blue line). The VBD errors are propagated from the standard deviations on each measured oxide and the analytical error on Fe (0.03) and S (0.05) oxidation states. If there was no measurement of Fe and/or S oxidation state, a value of 0.5±0.5 (i.e., unknown) was used. The black line indicates the 1-to-1 trend. Data available in the Supplementary Material.

6 Conclusions

Sub-surface charging is an important process to consider during EPMA of insulating materials, especially hydrous silicate glass, due to its effect on quantitative analysis (Cazaux, 1996). Sub-surface charging causes element migration and redox changes during analysis (e.g., Hughes et al., 2018; Humphreys et al., 2006; Zhang et al., 2018). Our Win X-ray modelling shows that sub-surface charging can also have a measurable effect on X-ray generation and emission, resulting in low analytical totals and high VBD contents. The ~1 wt.% overestimation of volatiles, predominantly H_2O, observed in the literature data when hydrous glass contains >2 wt.% volatiles, could cause a 50 MPa overestimation of the entrapment pressures of melt inclusions (Newman and Lowenstern, 2002), often used to decipher the architecture of volcano plumbing systems (e.g., Blundy and Cashman, 2008), resulting in ~ 2 km depth change which is on the order of the resolution of geophysical observations for shallow magma chambers (e.g., Field et al., 2012). The same issue would also cause an order of magnitude underestimation in the viscosity (e.g., Di Genova et al., 2013), which could change the inferred flow regime (e.g., Turner and Campbell, 1986), fragmentation mechanism (e.g., Namiki and Manga, 2008; Zhang, 1999), and whether the melt remained coupled to entrained bubbles and crystals (e.g., Jaupart and Vergniolle, 1988). Using an empirical correction to correct VBD removes the systematic overestimation of volatiles, and provides accurate volatile contents using EPMA.

This makes EPMA a useful, low-cost alternative to other techniques such as FTIR, SIMS and Raman, for analysis of volatiles at high spatial resolution, using a more readily available analytical instrument that does not suffer from problems due to fluorescence and nanolites.

Acknowledgements

We would like to thank David Neave (Leibniz Universität) for the R script used to calculate glass density. ECH is supported by a NERC GW4+ DTP studentship from the Natural Environment Research Council (NE/L002434/1) and is thankful for the support and additional funding from CASE partner GNS Science, New Zealand. GK acknowledges support from the New Zealand Strategic Science Investment Fund. We would like to thank Michael Stock and an anonymous reviewer for their helpful comments which greatly improved the manuscript, and Balz Kamber for his editorial handling of the manuscript.

References

Bastin, G.., Heijligers, H.J.M., 1991. Electron probe quantification. Plenum Press, New York.

Benhayoune, H., Jbara, O., 1996. Some experimental evidence for the Φ(0) variation in EPMA of insulating materials. X-Ray Spectrom. 25, 229–232. doi:10.1002/(SICI)1097-4539(199609)25:5<229::AID-XRS170>3.0.CO;2-\#

Blundy, J.D., Cashman, K.V., 2008. Petrologic reconstruction of magmatic system variables and processes. Rev. Mineral. Geochemistry 69, 179–239.

Blundy, J.D., Cashman, K.V., Rust, A., Witham, F., 2010. A case for CO2-rich arc magmas. Earth Planet. Sci. Lett. 290, 289–301. doi:10.1016/j.epsl.2009.12.013

Bonnelle, C., 2004. Charge trapping in dielectrics. Microsc. Microanal. 10, 691–696. doi:10.1017/S1431927604040620

Botcharnikov, R.E., Almeev, R.R., Koepke, J., Holtz, F., 2008. Phase relations and liquid lines of descent in hydrous ferrobasalt: Implications for the Skaergaard Intrusion and Columbia River Flood Basalts. J. Petrol. 49, 1687–1727. doi:10.1093/petrology/egn043

Botcharnikov, R.E., Koepke, J., Holtz, F., McCammon, C.A., Wilke, M., 2005. The effect of water activity on the oxidation and structural state of Fe in a ferro-basaltic melt. Geochim. Cosmochim. Acta 69, 5071–5085. doi:10.1016/j.gca.2005.04.023

Bottinga, Y., Weill, D.F., 1970. Densities of liquid silicate systems calculated from partial molar volumes of oxide components. Am. J. Sci. 269, 169–182.

Carmisciano, S., Rosa, I.M. De, Sarasini, F., Tamburrano, A., Valente, M., 2011. Basalt woven fiber reinforced vinylester composites: Flexural and electrical properties. Mater. Des. 32, 337–342. doi:10.1016/J.MATDES.2010.06.042

Cazaux, J., 1996. Electron probe microanalysis of insulating materials: Quantification problems and some possible solutions. X-Ray Spectrom. 25, 265–280. doi:10.1002/(SICI)1097-4539(199611)25:6<265::AID-XRS172>3.0.CO;2-3

Chabiron, A., Alyoshin, A.P., Cuney, M., Deloule, E., Golubev, V.N., Velitchkin, V.I., Poty, B., 2001. Geochemistry of the rhyolitic magmas from the Streltsovka caldera (Transbaikalia, Russia): A melt inclusion study. Chem. Geol. 175, 273–290. doi:10.1016/S0009-2541(00)00300-4

Cherifi, A., Dakka, M.A., Toureille, A., 1992. The validation of the thermal step method. IEEE Trans. Electr. Insul. 27, 1152–1158. doi:10.1109/14.204866

Cottrell, E., Kelley, K.A., 2011. The oxidation state of Fe in MORB glasses and the oxygen fugacity of the upper mantle. Earth Planet. Sci. Lett. 305, 270–282. doi:10.1016/j.epsl.2011.03.014

Delaney, J.R., Karsten, J.L., 1981. Ion microprobe studies of water in silicate melts: Concentration-dependent water diffusion in obsidian. Earth Planet. Sci. Lett. 52, 191–202. doi:10.1016/0012-821X(81)90220-X

Demers, H., Gauvin, R., 2004. X-ray microanalysis of a coated nonconductive specimen: Monte Carlo simulation. Microsc. Microanal. 10, 776–782. doi:https://doi.org/10.1017/S1431927604040607

Devine, J.D., Gardner, J.E., Brack, H.P., Laynet, G.D., Rutherford, M.J., 1995. Comparison of microanalytical methods for estimating H2O contents of silicic volcanic glasses. Am. Mineral. 80, 319–328.

Di Carlo, I., Pichavant, M., Rotolo, S.G., Scaillet, B., 2006. Experimental Crystallization of a High-K Arc Basalt: the Golden Pumice, Stromboli Volcano (Italy). J. Petrol. 47, 1317–1343. doi:10.1093/petrology/egl011

Di Genova, D., Hess, K.U., Chevrel, M.O., Dingwell, D.B., 2016. Models for the estimation of Fe3+/Fetot ratio in terrestrial and extraterrestrial alkali- and iron-rich silicate glasses using Raman spectroscopy. Am. Mineral. 101, 943–952. doi:https://doi.org/10.2138/am-2016-5534CCBYNCND

Di Genova, D., Kolzenburg, S., Wiesmaier, S., Dallanave, E., Neuville, D.R., Hess, K.U., Dingwell, D.B., 2017a. A compositional tipping point governing the mobilization and eruption style of rhyolitic magma. Nature 552, 235–238. doi:10.1038/nature24488

Di Genova, D., Romano, C., Giordano, D., Alletti, M., 2014. Heat capacity, configurational heat capacity and fragility of hydrous magmas. Geochim. Cosmochim. Acta 1, 314–333. doi:https://doi.org/10.1016/j.gca.2014.07.012

Di Genova, D., Romano, C., Hess, K.U., Vona, A., Poe, B.T., Giordano, D., Dingwell, D.B., Behrens, H., 2013. The rheology of peralkaline rhyolites from Pantelleria Island. J. Volcanol. Geotherm. Res. 249, 201–216. doi:10.1016/j.jvolgeores.2012.10.017

Di Genova, D., Sicola, S., Romano, C., Vona, A., Fanara, S., Spina, L., 2017b. Effect of iron and nanolites on Raman spectra of volcanic glasses: A reassessment of existing strategies to estimate the water content. Chem. Geol. 475, 76–86. doi:10.1016/J.CHEMGEO.2017.10.035

Donovan, J.J., Tingle, T.N., 1996. An improved mean atomic number background correction for quantitative microanalysis. Microsc. Microanal. 2, 1–7.

Donovan, J.J., Vicenzi, E.P., 2008. Water by EPMA- New developments. Microsc. Microanal. 14, 1274–1275.

Drew, D.L., Bindeman, I.N., Loewen, M.W., Wallace, P.J., 2016. Initiation of large-volume silicic centers in the Yellowstone hotspot track: insights from H2O- and F-rich quartz-hosted rhyolitic melt inclusions in the Arbon Valley Tuff of the Snake River Plain. Contrib. to Mineral. Petrol. 171, 10. doi:10.1007/s00410-015-1210-z

Erdmann, M., Koepke, J., 2016. Silica-rich lavas in the oceanic crust: experimental evidence for fractional crystallization under low water activity. Contrib. to Mineral. Petrol. 171, 83. doi:10.1007/s00410-016-1294-0

Fakhfakh, S., Jbara, O., Belhaj, M., Fakhfakh, Z., Kallel, A., Rau, E.I., 2003. An experimental approach for dynamic investigation of the trapping properties of glass-ceramic under electron beam irradiation from a scanning electron microscope. Eur. Phys. J. Appl. Phys. 21, 137–146. doi:10.1051/epjap:2003001

Fakhfakh, S., Jbara, O., Rondot, S., Hadjadj, A., Patat, J.M., Fakhfakh, Z., 2010. Analysis of electrical charging and discharging kinetics of different glasses under electron irradiation in a scanning electron microscope. J. Appl. Phys. 108, 093705. doi:10.1063/1.3499692

Faure, F., Schiano, P., 2005. Experimental investigation of equilibration conditions during forsterite growth and melt inclusion formation. Earth Planet. Sci. Lett. 236, 882–898. doi:10.1016/J.EPSL.2005.04.050

Feig, S.T., Koepke, J., Snow, J.E., 2006. Effect of water on tholeiitic basalt phase equilibria: an experimental study under oxidizing conditions. Contrib. to Mineral. Petrol. 152, 611–638. doi:10.1007/s00410-006-0123-2

Field, L., Blundy, J.D., Brooker, R.A., Wright, T., Yirgu, G., 2012. Magma storage conditions beneath Dabbahu Volcano (Ethiopia) constrained by petrology, seismicity and satellite geodesy. Bull. Volcanol. 74, 981–1004. doi:10.1007/s00445-012-0580-6

Gaillard, F., Scaillet, B., Pichavant, M., Bény, J., 2001. The effect of water and fO2 on the ferric–ferrous ratio of silicic melts. Chem. Geol. 174, 255–273. doi:10.1016/S0009-2541(00)00319-3

Gauvin, R., Lifshin, E., Demers, H., Horny, P., Campbell, H., 2006. Win X-ray: A new Monte Carlo program that computes X-ray spectra obtained with a scanning electron microscope. Microsc. Microanal. 12, 49–64.

Gedeon, O., Jurek, K., 2002. Decay curve analysis of alkali-silicate glass exposed to electrons. Microchim. Acta 139, 67–70. doi:10.1007/s006040200041

Gedeon, O., Jurek, K., Hulínský, V., 1999. Fast migration of alkali ions in glass irradiated by electrons. J. Non. Cryst. Solids 246, 1–8. doi:10.1016/S0022-3093(99)00083-6

Ghorbel, N., Fakhfakh, S., Jbara, O., Odof, S., Rondot, S., Fakhfakh, Z., Kallel, A., 2005. EPMA analysis of insulating materials: Monte Carlo simulations and experiments. J. Phys. D. Appl. Phys. 38, 1239–1247. doi:10.1088/0022-3727/38/8/022

Giordano, D., Dingwell, D., 2003. Viscosity of hydrous Etna basalt: implications for Plinian-style basaltic eruptions. Bull. Volcanol. 65, 8–14. doi:10.1007/s00445-002-0233-2

Gurenko, A.A., Trumbull, R.B., Thomas, R., Lindsay, J.M., 2005. A melt inclusion record of

volatiles, trace elements and Li-B isotope variations in a single magma system from the Plat Pays Volcanic Complex, Dominica, Lesser Antilles. J. Petrol. 46, 2495–2526. doi:10.1093/petrology/egi063

Hauri, E.H., Wang, J., Dixon, J.E., King, P.L., Mandeville, C., Newman, S., 2002. SIMS analysis of volatiles in silicate glasses. Chem. Geol. 183, 99–114. doi:10.1016/S0009-2541(01)00375-8

Holtz, F., Sato, H., Lewis, J., Behrens, H., Nakada, S., 2004. Experimental petrology of the 1991-1995 Unzen dacite, Japan. Part I: Phase relations, phase composition and pre-eruptive conditions. J. Petrol. 46, 319–337. doi:10.1093/petrology/egh077

Hughes, E.C., Buse, B., Kearns, S.L., Blundy, J.D., Kilgour, G., Mader, H.M., Brooker, R.A., Blazer, B., Botcharnikov, R.E., Di Genova, D., Almeev, R.R., Riker, J.M., 2018. High spatial resolution analysis of the Iron oxidation state in silicate glasses using the electron probe. Am. Mineral.

Humphreys, M.C.S., Kearns, S.L., Blundy, J.D., 2006. SIMS investigation of electron-beam damage to hydrous, rhyolitic glasses: Implications for melt inclusion analysis. Am. Mineral. 91, 667–679. doi:10.2138/am.2006.1936

Jaupart, C., Vergniolle, S., 1988. Laboratory models of Hawaiian and Strombolian eruptions. Nature 331, 58–60. doi:10.1038/331058a0

Jbara, O., Cazaux, J., Trebbia, P., 1995. Sodium diffusion in glasses during electron irradiation. J. Appl. Phys. 78, 868–875. doi:10.1063/1.360277

Jbara, O., Fakhfakh, S., Belhaj, M., Cazaux, J., Rau, E.I., Filippov, M., Andrianov, M.V., 2002. A new experimental approach for characterizing the internal trapped charge and electric field build up in ground-coated insulators during their e− irradiation. Nucl. Instruments Methods Phys. Res. Sect. B Beam Interact. with Mater. Atoms 194, 302–310. doi:10.1016/S0168-583X(02)00666-3

Jbara, O., Fakhfakh, S., Belhaj, M., Rondot, S., 2004. Charge implantation measurement on electron-irradiated insulating materials by means of a SEM technique. Microsc. Microanal. 10, 697–710.

Jbara, O., Portron, B., Mouze, D., Cazaux, J., 1997. Electron probe microanalysis of insulating oxides: Monte Carlo simulations. X-Ray Spectrom. 26, 291–302. doi:10.1002/(SICI)1097-4539(199709)26:5<291::AID-XRS226>3.0.CO;2-X

Kanaya, K., Okayama, S., Mouze, D., Cazaux, J., Ferrier, R.P., 1972. Penetration and energy-loss theory of electrons in solid targets. J. Phys. D. Appl. Phys. 5, 308. doi:10.1088/0022-3727/5/1/308

Kelley, K.A., Cottrell, E., 2009. Water and the oxidation state of subduction zone magmas. Science (80-.). 325, 605–7. doi:10.1126/science.1174156

Kent, A.J.R., 2008. Melt Inclusions in Basaltic and Related Volcanic Rocks. Rev. Mineral. Geochemistry 69, 273–331.

King, P.L., Vennemann, T.W., Holloway, J.R., Hervig, R.L., Lowenstern, J.B., Forneris, J.F., 2002. Analytical techniques for volatiles: A case study using intermediate (andesitic) glasses. Am. Mineral. 87, 1077–1089. doi:https://doi.org/10.2138/am-2002-8-904

Lange, R.A., 1997. A revised model for the density and thermal expansivity of K2O-

Na2<\sub>O-CaO-MgO-Al2O3-SiO2 liquids from 700 to 1900 K: extension to crustal magmatic temperatures. Contrib. to Mineral. Petrol. 130, 1–11. doi:10.1007/s004100050345

Lange, R.L., Carmichael, I.S.E., 1990. Thermodynamic properties of silicate liquids with emphasis on density, thermal expansion and compressibility. Rev. Mineral. Geochemistry 24, 25–64.

Lesne, P., Kohn, S.C., Blundy, J.D., Witham, F., Botcharnikov, R.E., Behrens, H., 2011. Experimental Simulation of Closed-System Degassing in the System Basalt-H2O-CO2-S-Cl. J. Petrol. 52, 1737–1762. doi:10.1093/petrology/egr027

Lineweaver, J.L., 1963. Oxygen outgassing caused by electron bombardment of glass. J. Appl. Phys. 34, 1786. doi:https://doi.org/10.1063/1.1702680

Maeno, T., Hoshino, T., Futami, T., Takada, T., 1989. Application of ultrasonic techniques to the measurement of spatial charge and electric field distributions in solid dielectric materials. Electr. Eng. Japan 109, 58–64. doi:10.1002/eej.4391090507

Melekhova, E., Blundy, J.D., Robertson, R., Humphreys, M.C.S., 2015. Experimental evidence for polybaric differentiation of primitive arc basalt beneath St. Vincent, Lesser Antilles. J. Petrol. 56, 161–192. doi:10.1093/petrology/egu074

Métrich, N., Allard, P., Spilliaert, N., Andronico, D., Burton, M.R., 2004. 2001 flank eruption of the alkali- and volatile-rich primitive basalt responsible for Mount Etna's evolution in the last three decades. Earth Planet. Sci. Lett. 228, 1–17. doi:10.1016/J.EPSL.2004.09.036

Métrich, N., Wallace, P.J., 2009. Volatile Abundances in Basaltic Magmas and Their Degassing Paths Tracked by Melt Inclusions. Rev. Mineral. Geochemistry 69.

Michael, P.J., Cornell, W.C., 1998. Influence of spreading rate and magma supply on crystallization and assimilation beneath mid-ocean ridges: Evidence from chlorine and major element chemistry of mid-ocean ridge basalts. J. Geophys. Res. Solid Earth 103, 18325–18356. doi:10.1029/98JB00791

Morgan, G.B., London, D., 2005. Effect of current density on the electron microprobe analysis of alkali aluminosilicate glasses. Am. Mineral. 90, 1131–1138. doi:https://doi.org/10.2138/am.2005.1769

Namiki, A., Manga, M., 2008. Transition between fragmentation and permeable outgassing of low viscosity magmas. J. Volcanol. Geotherm. Res. 169, 48–60.

Nash, W.P., 1992. Analysis of oxygen with electron microprobe: Applications to hydrated glass and minerals. Am. Mineral. 77, 453–457.

Naumov, V.B., 2011. Rhyolitic melts in eastern Transbaikalia and the North Caucasus: chemical composition, volatiles, and admixture elements (from data of study of melt inclusions in minerals). Russ. Geol. Geophys. 52, 1368–1377. doi:10.1016/j.rgg.2011.10.008

Naumov, V.B., Tolstykh, M.L., Grib, E.N., Leonov, V.L., Kononkova, N.N., 2008. Chemical composition, volatile components, and trace elements in melts of the Karymskii volcanic center, Kamchatka, and Golovnina volcano, Kunashir Island: Evidence from inclusions in minerals. Petrology 16, 1–18. doi:10.1134/S0869591108010013

Newman, S., Lowenstern, J.B., 2002. VolatileCalc: a silicate melt–H2O–CO2 solution model written in Visual Basic for excel. Comput. Geosci. 28, 597–604. doi:10.1016/S0098-3004(01)00081-4

Newman, S., Stolper, E.M., Epstein, S., 1986. Measurement of water in rhyolitic glasses: Calibration of an infrared spectroscopic technique. Am. Mineral. 71, 1527–1541.

Nichols, A.R.L., Carroll, M.R., Höskuldsson, Á., 2002. Is the Iceland hot spot also wet? Evidence from the water contents of undegassed submarine and subglacial pillow basalts. Earth Planet. Sci. Lett. 202, 77–87. doi:10.1016/S0012-821X(02)00758-6

Nielsen, C.H., Sigurdsson, H., 1981. Quantitative methods for electron microprobe analysis of sodium in natural and synthetic glasses. Am. Mineral. 66, 547–552.

Ochs, F.A., Lange, R.A., 1999. The density of hydrous magmatic liquids. Science (80-.). 283, 1314–1317. doi:10.1126/science.283.5406.1314

Putirka, K.D., 2008. Thermometers and Barometers for Volcanic Systems. Rev. Mineral. Geochemistry 69, 61–120. doi:10.2138/rmg.2008.69.3

Riker, J.M., Blundy, J.D., Rust, A.C., Botcharnikov, R.E., Humphreys, M.C.S., 2015. Experimental phase equilibria of a Mount St. Helens rhyodacite: A framework for interpreting crystallization paths in degassing silicic magmas. Contrib. to Mineral. Petrol. 170. doi:doi:10.1007/s00410-015-1160-5

Roeder, P.L., Emslie, R.F., 1970. Olivine-liquid equilibrium. Contrib. to Mineral. Petrol. 29, 275–289. doi:10.1007/BF00371276

Roman, D.C., Cashman, K.V., Gardner, C.A., Wallace, P.J., Donovan, J.J., 2006. Storage and interaction of compositionally heterogeneous magmas from the 1986 eruption of Augustine Volcano, Alaska. Bull. Volcanol. 68, 240–254. doi:10.1007/s00445-005-0003-z

Rutherford, M.J., Devine, J.D., 1996. Preeruption pressure-temperature conditions and volatiles in the 1991 dacitic magma of Mount Pinatubo. Fire mud eruptions lahars Mt. Pinatubo, Philipp. 751–766.

Sessler, G.M., Yang, G.M., 1998. Materials for Advanced Metallization, in: MAM ’97 Abstracts Booklet., European Workshop. Société française du vide, pp. 38–47.

Shorttle, O., Moussallam, Y., Hartley, M.E., Maclennan, J., Edmonds, M., Murton, B.J., 2015. Fe-XANES analyses of Reykjanes Ridge basalts: Implications for oceanic crust’s role in the solid Earth oxygen cycle. Earth Planet. Sci. Lett. 427, 272–285. doi:10.1016/j.epsl.2015.07.017

Smith, V.C., Shane, P., Nairn, I.A., 2010. Insights into silicic melt generation using plagioclase, quartz and melt inclusions from the caldera-forming Rotoiti eruption, Taupo volcanic zone, New Zealand. Contrib. to Mineral. Petrol. 160, 951–971. doi:10.1007/s00410-010-0516-0

Sommer, M.A., 1977. Volatiles H2O, CO2, and CO in Silicate Melt Inclusions in Quartz Phenocrysts from the Rhyolitic Bandelier Air-Fall and Ash-Flow Tuff, New Mexico. J. Geol. 85, 423–432. doi:10.1086/628316

Stamper, C.C., Melekhova, E., Blundy, J.D., Arculus, R.J., Humphreys, M.C.S., Brooker, R.A., 2014. Oxidised phase relations of a primitive basalt from Grenada, Lesser Antilles.

Contrib. to Mineral. Petrol. 167, 954. doi:10.1007/s00410-013-0954-6

Stock, M.J., Humphreys, M.C.S., Smith, V.C., Johnson, R.D., Pyle, D.M., 2015. New constraints on electron-beam induced halogen migration in apatite. Am. Mineral. 100, 281–293. doi:10.2138/am-2015-4949

Thomas, R., 2000. Determination of water contents of granite melt inclusions by confocal laser Raman microprobe spectroscopy. Am. Mineral. 85, 868–872. doi:10.2138/am-2000-5-631

Toplis, M.J., Dingwell, D.B., Libourel, G., 1994. The effect of phosphorus on the iron redox ratio, viscosity, and density of an evolved ferro-basalt. Contrib. to Mineral. Petrol. 117, 293–304. doi:10.1007/BF00310870

Turner, J.S., Campbell, I.H., 1986. Convection and mixing in magma chambers. Earth-Science Rev. 23, 255–352. doi:10.1016/0012-8252(86)90015-2

Webster, J.D., Burt, D.M., Aguillon, R.A., 1996. Volatile and lithophile trace-element geochemistry of Mexican tin rhyolite magmas deduced from melt inclusions. Geochim. Cosmochim. Acta 60, 3267–3283. doi:10.1016/0016-7037(96)00163-9

Webster, J.D., Congdon, R.D., Lyons, P.C., 1995. Determining pre-eruptive compositions of late Paleozoic magma from kaolinized volcanic ashes: Analysis of glass inclusions in quartz microphenocrysts from tonsteins. Geochim. Cosmochim. Acta 59, 711–720. doi:10.1016/0016-7037(94)00356-Q

Webster, J.D., Duffield, W.A., 1991. Volatiles and lithophile elements in Taylor Creek Rhyolite: Constraints from glass inclusion analysis. Am. Mineral. 76, 1628–1645.

Wilke, M., Behrens, H., Burkhard, D.J.., Rossano, S., 2002. The oxidation state of iron in silicic melt at 500 MPa water pressure. Chem. Geol. 189, 55–67. doi:10.1016/S0009-2541(02)00042-6

Zhang, C., Almeev, R.R., Hughes, E.C., Borisov, A., Wolff, E., Hofer, H.E., Botcharnikov, R.E., Koepke, J., 2018. Electron microprobe technique for the determination of iron oxidation state in silicate glasses. Am. Mineral. 103, 1445–1454.

Zhang, Y., 1999. A criterion for the fragmentation of bubbly magma based on brittle failure theory. Nature 402, 648–650. doi:10.1038/45210

Zhang, Y., Belcher, R., Ihinger, P.D., Wang, L., Xu, Z., Newman, S., 1997. New calibration of infrared measurement of dissolved water in rhyolitic glasses. Geochim. Cosmochim. Acta 61, 3089–3100. doi:10.1016/S0016-7037(97)00151-8